Complexity and simplicity of optimal control theory pulses shaped for controlling vibrational qubits

Dmytro Shyshlov and Dmitri Babikov

Citation: J. Chem. Phys. **137**, 194318 (2012); doi: 10.1063/1.4765344
View online: http://dx.doi.org/10.1063/1.4765344
View Table of Contents: http://jcp.aip.org/resource/1/JCPSA6/v137/i19
Published by the AIP Publishing LLC.

Complexity and simplicity of optimal control theory pulses shaped for controlling vibrational qubits

Dmytro Shyshlov and Dmitri Babikov[a)]
Department of Chemistry, Marquette University, PO Box 1881, Milwaukee, Wisconsin 53201, USA

(Received 17 August 2012; accepted 18 October 2012; published online 21 November 2012)

In the context of molecular quantum computation the optimal control theory (OCT) is used to obtain shaped laser pulses for high-fidelity control of vibrational qubits. Optimization is done in time domain and the OCT algorithm varies values of electric field in each time step independently, tuning hundreds of thousands of parameters to find one optimal solution. Such flexibility is not available in experiments, where pulse shaping is done in frequency domain and the number of "tuning knobs" is much smaller. The question of possible experimental interpretations of theoretically found OCT solutions arises. In this work we analyze very accurate optimal pulse that we obtained for implementing quantum gate CNOT for the two-qubit system encoded into the exited vibrational states of thiophosgene molecule. Next, we try to alter this pulse by reducing the number of available frequency channels and intentionally introducing systematic and random errors (in frequency domain, by modifying the values of amplitudes and phases of different frequency components). We conclude that a very limited number of frequency components (only 32 in the model of thiophosgene) are really necessary for accurate control of the vibrational two-qubit system, and such pulses can be readily constructed using OCT. If the amplitude and phase errors of different frequency components do not exceed $\pm 3\%$ of the optimal values, one can still achieve accurate transformations of the vibrational two-qubit system, with gate fidelity of CNOT exceeding 0.99. © *2012 American Institute of Physics*. [http://dx.doi.org/10.1063/1.4765344]

I. INTRODUCTION

It is often argued that shaped laser pulses, prepared theoretically using the optimal control theory (OCT), would be hard or even impossible to reproduce in experiments. In such calculations, the OCT pulse "shaping" is carried out in the time domain with the number of "tuning knobs" equal to the number of time steps within the total pulse duration.[1–3] For example, for a 25 ps laser pulse the number of time steps (used for accurate propagation of time-dependent Schrödinger equation and optimization of pulse's shape) may be close to 2^{20}.[4] Indeed, such flexibility is usually unavailable in experiments,[5–7] where the number of frequency channels never exceeds 2^{10}. For this reason it is sometimes suggested that theoreticians migrate from the OCT methods towards the evolutionary genetic algorithms[8–10] that, similar to experiments, carry out pulse optimization in the frequency domain.

In this paper, using standard techniques of Fourier transform, we show that the OCT pulses, seemingly complicated in time domain, are in fact very simple in the frequency domain. We demonstrate by calculations that a very accurate pulse, optimized in time domain for coherent manipulation of vibrational states of the molecule, can be reproduced surprisingly well using as few as 2^5 frequency channels. This is well within the reach of today's pulse shaping techniques, which justifies the use of OCT method as a predictive practical tool.

Another focus of this paper is on robustness of the OCT solutions. It is sometimes argued that such pulses are very fragile, so that changing the pulse shape just slightly would change dramatically the result of action of the pulse on a molecule. In our numerical experiments we take a very accurate OCT pulse and modify it in several different ways, using filters in the frequency domain. The effect of modification is then studied by acting, with the modified pulse, on a molecule.

The issues of accuracy, reproducibility and robustness are particularly important in context of molecular quantum computing (QC),[11–32] where the requirements to fidelity of state-to-state transformations are very high. Thus, the examples studied here are drawn from the field of quantum information processing with vibrational qubits, where the optimized laser pulses are used to manipulate vibrational wave packets coherently, providing the desired unitary transformations of qubit states. For these cases, the effects of systematic and random errors of pulse shaping are studied.

This paper is organized as follows. In Sec. II we describe in detail the physical model of vibrational quantum computer. Section III gives details of OCT pulse preparation. Results are presented and discussed in Sec. IV. Section V summarized major findings of this work.

II. THE MODEL SYSTEM AND QUANTUM GATES

We use vibrational eigenstates of thiophosgene ($SCCl_2$) to encode qubits. Vibrational spectrum and dipole moment matrix of this molecule are known from the experiment.[33] We

a)Author to whom correspondence should be addressed. Electronic mail: Dmitri.Babikov@mu.edu.

TABLE I. Relevant vibrational energy levels and transition dipole moments of $SCCl_2$ molecule.

Energy (cm^{-1})	Dipole moment (Debye)	Two-qubit assignment
8191.03	0.44	...
8239.53	0.36	...
8246.35	0.38	$\|00\rangle$
8264.26	0.96	$\|01\rangle$
8273.98	0.75	$\|10\rangle$
8278.82	0.70	$\|11\rangle$
8292.89	0.61	...
8319.93	0.43	...

focus on 28 vibrational eigenstates in energy range from 8032 to 8493 cm^{-1}. Four states close to the center of this interval, in the range from 8246 to 8279 cm^{-1}, are used to encode two qubits (computing states) but the remaining 24 states are also included in optimization in order to ensure that no population is transferred to other vibrational states (interfering states). Also, including all 28 vibrational states, in a ~450 cm^{-1} energy range, provide a realistic description of this physical system.

In the model of quantum computer considered here there is no direct population transfer between the computational states. Instead, all transitions go through the electronically exited state at energy 35 125 cm^{-1}, the gateway state referenced further as $|G\rangle$. This choice allows using laser pulses in the UV/vis range and makes experimental realization of this scenario possible, based on mature pulse shaping technology.[34–37] Table I gives energies and dipole moments for the most important states in our calculations. This includes four states of the two-qubit system and two interfering states, energetically closest to the computing states. Assignments of the qubit states are also given in Table I. Energies and dipole moments of the remaining states can be found in Ref. 8.

Large number of vibrational eigenstates in thiphosgene makes it feasible to implement multi-qubit quantum gates or even simple quantum algorithms.[8] Here we focus on two-qubit gate CNOT (conditional NOT) which plays a very important role in quantum computation.[38] The action of this gate can be described as follows: If the first qubit (the control qubit) is in state $|0\rangle$ then the second qubit (the target qubit) is left unchanged but, if the first qubit is in state $|1\rangle$ then the state of second qubit is flipped. In a concise form this can be written as

$$\text{CNOT}\ |00\rangle \rightarrow |00\rangle\,, \tag{1a}$$

$$\text{CNOT}\ |01\rangle \rightarrow |01\rangle\,, \tag{1b}$$

$$\text{CNOT}\ |10\rangle \rightarrow |11\rangle\,, \tag{1c}$$

$$\text{CNOT}\ |11\rangle \rightarrow |10\rangle\,. \tag{1d}$$

As explained in Sec. III, the laser field is optimized such that a single universal pulse is capable of carrying out each of these four transitions. Which one is actually performed, depends only on the initial state of the molecule. It should also be remembered that quantum system can be in any superposition of these states, and the laser pulse should be able to transform appropriately the superposition state as well. This is achieved by optimizing, in addition to four transitions above, the action of quantum gate onto an equally weighted superposition of qubit states,

$$\text{CNOT}\frac{1}{2}\left(|00\rangle + |01\rangle + |10\rangle + |11\rangle\right) \rightarrow \frac{1}{2}\left(|00\rangle + |01\rangle + |10\rangle + |11\rangle\right). \tag{2}$$

It has been demonstrated that, if all five transitions are optimized simultaneously, the common phase is enforced for all transitions and the resultant laser pulse is indeed capable of carrying out a unitary and coherent transformation of any arbitrarily chosen qubit state.[16,39]

In practice, when optimization is never perfect, the accuracy of optimized pulse can be characterized by computing the average transition probability,

$$P = \frac{1}{K}\sum_{k=1}^{K} |\langle\varphi_f|\psi(T)\rangle|^2. \tag{3}$$

Each term of this sum represents an overlap of the actual laser driven wave function $\psi(T)$ at the final moment of time T with the desirable perfect final state φ_f. Summation is over the set of transitions optimized simultaneously. For optimization of the phase-corrected CNOT gate $K = 5$, as discussed above. Another quality used to assess the optimized pulse is gate fidelity,

$$F = \frac{1}{K^2}\left|\sum_{k=1}^{K}\langle\varphi_f|\psi(T)\rangle\right|^2. \tag{4}$$

Note that in this expression different overlaps are added coherently, which takes into account the phase information. If the final phases of different optimized transitions are not perfectly aligned, the value of F can be low, even if the value of phase-insensitive P is high. Thus, monitoring F guaranties and is usually done in conjunction with adding the fifth transition, Eq. (2), to the set of optimized transitions.

Our prior experience with this system and with other models of the vibrational quantum computer[40–43] tells that the multi-qubit conditional gate CNOT is usually the hardest to optimize. If this gate is optimized and the result is satisfactory, then the other one-qubit quantum gates (such as unconditional NOT gate, the phase rotation gate, and the Hadamard gate[38]) are relatively easy to optimize. So, in this paper we focus on the CNOT gate only. It is worth mentioning that experimental demonstration of this one quantum gate would make a very important impact on the field of molecular QC, as it did in case of the ion-trap quantum computer.[44,45]

III. OCT PULSE OPTIMIZATION

We implement the multi-target version of the OCT as follows. We maximize the following functional:

$$\Im \equiv \sum_{k=1}^{K} |\langle \phi_f | \psi(T) \rangle|^2 - \alpha \int_0^T \frac{\varepsilon^2(t)}{s(t)} dt - \sum_{k=1}^{K} 2Re \left\{ \langle \phi_f | \psi(T) \rangle \int_0^T \langle \psi(t) | \frac{i}{\hbar} [\hat{H}_0 - \varepsilon(t)\mu] + \frac{\partial}{\partial t} | \psi(t) \rangle dt \right\} \quad (5)$$

with respect to variations in wave function $\psi(t)$ and the field $\varepsilon(t)$. The first term here is P from Eq. (3) and it is maximized. The second term represents energy of the laser field. It is minimized. Parameter α is a constant penalty factor and $s(t) = \sin^2(\pi \frac{t}{T})$ is a variable penalty function. The last term of the functional (5) is constructed in such a way that system's dynamics is restricted to obey the time-dependent Schrödinger equation, while the system is driven from the initial state ϕ_i towards the final state ϕ_f. Note that this functional is a multi-target version,[14,21] where the sum over k in the first and the last terms is taken over all optimized transitions, $1 \le k \le K$. Variations of this functional with respect to the wave function and the field, one obtains the following equations:[1,46] A set of K time-dependent Schrödinger equations propagated forward in time,

$$i\hbar \frac{\partial}{\partial t} \vec{\psi}(t) = [\hat{H}_0 - \mu \varepsilon(t)] \vec{\psi}(t), \quad (6)$$

each with its own boundary condition $\vec{\psi}(0) = \phi_i$. A set of K analogous equation propagated backward in time,

$$i\hbar \frac{\partial}{\partial t} \overleftarrow{\psi}(t) = [\hat{H}_0 - \mu \varepsilon(t)] \overleftarrow{\psi}(t), \quad (7)$$

each with its own boundary condition $\overleftarrow{\psi}(T) = \phi_f$. And one equation for the common field,

$$\varepsilon(t) = -\frac{s(t)}{\alpha} \sum_{k=1}^{K} Im \langle \vec{\psi}(t) | \overleftarrow{\psi}(t) \rangle \langle \overleftarrow{\psi}(t) | \mu | \vec{\psi}(t) \rangle, \quad (8)$$

which uses information obtained from all these $2K$ equations. In order to propagate the Schrödinger equation in time we use the basis set expansion with time-dependent coefficients $c_n(t)$,

$$\psi(x,t) = \sum_{n=1}^{N} c_n(t) \cdot \varphi_n(x) \cdot e^{-iE_n t}. \quad (9)$$

Here $\varphi_n(x)$ are eigenfunctions of the system and E_n are their corresponding energy eigenvalues. Substitution of this expansion into the time-dependent Schrödinger equation leads to the following equations for the coefficients $c_n(t)$:

$$\dot{c}_n^R(t) = \varepsilon(t) \sum_m \left(c_m^R(t) \sin\theta_{m,n} - c_m^I(t) \cos\theta_{m,n} \right) \cdot M_{m,n}, \quad (10a)$$

$$\dot{c}_n^I(t) = \varepsilon(t) \sum_m \left(c_m^R(t) \cos\theta_{m,n} - c_m^I(t) \sin\theta_{m,n} \right) \cdot M_{m,n}, \quad (10b)$$

where $\theta_{m,n} = (E_m - E_n)t$ are phase shifts, $M_{m,n} = \langle \psi_m | \mu | \psi_n \rangle$ are the elements of the dipole moment matrix, and c_m^R and c_m^I are real and imaginary parts of complex coefficient c_m.

Equations (6)–(8) are then solved iteratively. The number of basis states in the expansion of Eq. (5) was $N = 29$. Those were 28 vibrational states in the ground electronic state of thiophosgene plus the gateway state. They all were included in the wave function propagation. The Runge-Kutta method of 4th order was used to propagate Eqs. (10a) and (10b). We start with backward propagation using the guess field in the following simple analytic form: $\varepsilon(t) = A \cdot \sin\omega t \cdot \sin^2(\pi \frac{t}{T})$, where A is amplitude of the guess field. Frequency of the guess field is $\omega = E_G - \bar{E}$, where E_G is energy of the gateway state and $\bar{E}$ is energy in the middle of the spectrum ($\bar{E}$ =8269.12 cm^{-1}). During the backward propagation, the program calculates new values of the field for each time step and this updated field is then used for the forward propagation, and so on. The pulse duration was set to $T = 25$ ps. This time interval was divided into 300 000 time steps for the Runge-Kutta propagation. This number was chosen as a compromise between the computational time and norm conservation. Thus, the time step in our calculations is $\Delta t \approx 0.083$ fs. It was found that fidelity of propagation depends somewhat on the penalty factor α. Thus, several calculations were carried out with slightly different α values. Some of them were discarded. The "keeper" values follow: $\alpha = \{33.5, 34.7, 36.0, 37.1, 38.3, 40.1\}$.

IV. RESULTS AND ANALYSIS

We found that for all values of the penalty factor used the probability of qubit transformation is slightly higher than fidelity. This behavior is expected, since calculation of fidelity takes phases of optimized transitions into account, and some small remaining phase errors lead to slight reduction of fidelity.[38,39] All probabilities are within 7.2×10^{-5} of each other and the same is true for fidelities. The best results were obtained with $\alpha = 40.1$, namely: $P = 0.999905$ and $F = 0.999837$. We see that the value of average probability slightly exceeds 0.9999, while the value of fidelity almost reaches 0.9999. We also saw that after ~80 000 iterations (when optimization was stopped) both probability and fidelity were still increasing, so, one can assume that even higher values of P and F are achievable, given appropriate computational resources. In what follows, the best optimized pulse ($\alpha = 40.1$, $P = 0.999905$, $F = 0.999837$) is analyzed.

A. Analysis of unaltered optimized pulse

Shape of the optimized pulse $\varepsilon(t)$ is presented in Fig. 1. The field switches "on" and "off" smoothly, reaching the level of ~6×10^6V/m closer to the middle of the pulse. Although the frequency of the field is very high, and the peak-to-peak oscillations cannot be resolved in Fig. 1, the pulse envelope

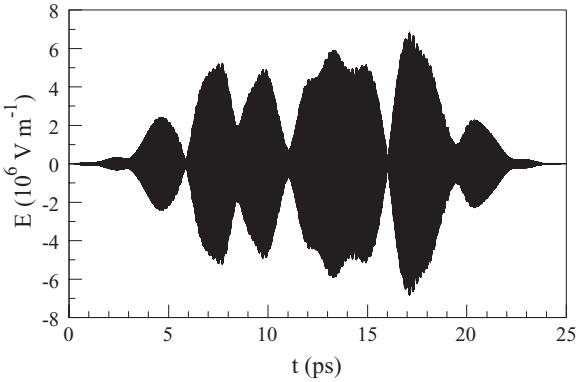

FIG. 1. Laser pulse optimally shaped for CNOT gate (time domain).

is relatively smooth. Overall, in time domain the pulse contains six clearly identified peaks, with only four dominant structures.

In order to analyze frequency content of the optimized pulse we used standard techniques of the FFT. In time domain our pulse consists of 300 001 points. The first point is at $t = 0$ and the last point is at $t = T$, where the field amplitude is exactly restricted to zero by means of the penalty function $s(t)$ as discussed above. The last point of the pulse was removed to ensure periodicity of the signal. The remaining 300 000 values of the field $\varepsilon(t)$ were used to define real parts of the complex signal. Imaginary parts of the complex signal were filled by zeros. This complex signal was Fourier transformed into the frequency domain, giving 150 000 independent positive frequency components from $v_{\min} = \Delta v = 1.35\,\text{cm}^{-1}$ to $v_{\max} = 200\,231\ \text{cm}^{-1}$ (and the corresponding 149 999 negative frequency components, plus one point at $v = 0$). The indicated value of $v_{\max}$ is very large, due to small time-propagation step Δt.

Discussion in Sec. IV B will emphasize that only the narrow part of spectrum (within the transition frequency range of the system) carries all physically relevant information. Indeed, first glance at the full frequency spectrum of the Fourier-transformed pulse shows that amplitudes of the frequency components that lie in the range $26\,850 \pm 40\ \text{cm}^{-1}$ are significantly higher than the rest of the spectrum. This part of spectrum is depicted in Fig. 1. The spectrum of optimized pulse is dominated by three peaks that closely correspond to transition frequencies between the gateway state and states $|01\rangle$, $|10\rangle$, and $|11\rangle$ of the two-qubit system (blue sticks). In contrast, near the frequency of transition to state $|00\rangle$ the amplitude is very small. This is understood, due to nature of the gate CNOT, expressed by Eq. (1). Namely, the result of acting with CNOT gate onto state $|00\rangle$ is to leave the qubit unchanged (see Eq. (1a)) and the trivial solution for that is to not disturb the population of this state. The OCT algorithm is capable of recognizing this, and excluding the frequency of $|G\rangle$-to-$|00\rangle$ transition from the pulse. Analysis of state populations during the pulse shows that, indeed, the optimized CNOT field hardly affects population of state $|00\rangle$. Even in the cases of other three optimized transitions, Eqs. (1b)–(1d), the population of state $|00\rangle$ remains unchanged (unpopulated in those cases) during the entire duration of the pulse.

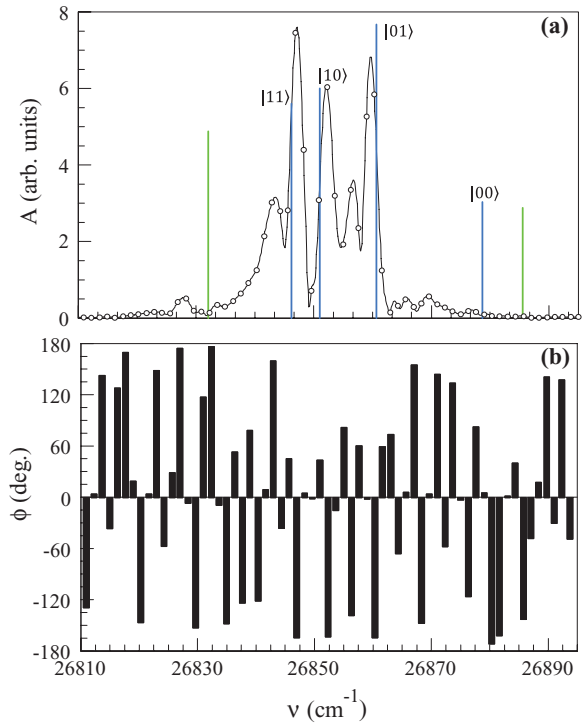

FIG. 2. Results of Fourier transform of the optimized pulse in the narrow frequency range (64 channels). Panel A shows amplitudes of frequency components. Four transition frequencies for computing states (molecular eigenstates used to encode two-qubit system) are indicated by blue sticks. Transition frequencies for two interfering eigenstates are also shown, by green sticks. Heights of these sticks are proportional to the corresponding transition dipole moments. Panel B shows phases of frequency components.

One could expect same behavior for state $|01\rangle$ since CNOT gate transforms this state into itself as well (see Eq. (1b)). However, Fig. 2 shows an intense peak at this frequency, and we found that population of state $|01\rangle$ is changing significantly during all four optimized transitions of Eq. (1), even during the seemingly trivial CNOT$|01\rangle \rightarrow |01\rangle$ transition. This happens because state $|01\rangle$ is energetically closer to states $|10\rangle$ and $|11\rangle$, and its dipole moment is the largest. As result, this transition interferes significantly with other optimized transitions. The OCT algorithm cannot exclude the corresponding frequency from the pulse, and has to optimize the transitions needed to control it. In contrast to this, state $|00\rangle$ discussed above lies furthest in energy and possesses smallest dipole moment (see Fig. 2).

Other features of spectrum in Fig. 2 include an intense broad wing on the low-frequency side, and a less intense wing on the high frequency side. Note, however, that the frequencies of transitions to the interfering states (green sticks) are completely suppressed by the OCT pulse optimization.

Finally, we looked at dynamics of population transfer between the qubit states during action of the optimized pulse. Here we will analyze in detail one of the optimized transitions, CNOT$|10\rangle \rightarrow |11\rangle$, see Eq. (1c). During this process state populations evolve very similar to what is illustrated in Fig. 3. From this figure one can notice that state populations change smoothly, despite highly oscillatory behavior of the electric field of the pulse applied to the molecule (compare to Fig. 1). The population dynamics is not entirely monotonic,

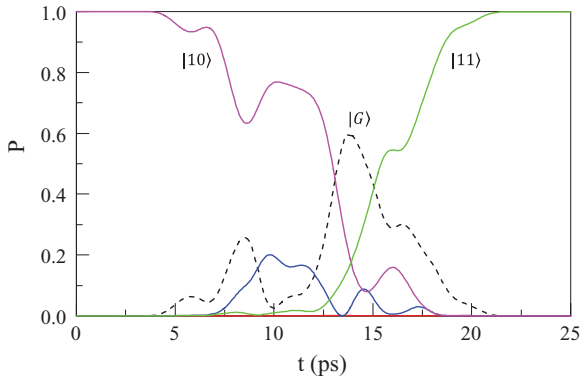

FIG. 3. Dynamics of state populations during transformation CNOT|10⟩ → |11⟩ of the two-qubit system. The case of 32 frequency channels is shown.

with some populations going up and down, but the overall picture is quite transparent. Figure 3 shows that during the initial ∼3 ps, when the field smoothly rises, the populations stay almost constant. Next, we observe the transfer of population from the initial state |10⟩ into the gateway state |G⟩. In the middle of the pulse population of |G⟩ reaches ∼0.6. At this point the population of target state |11⟩ starts increasing (due to transfer from the gateway state) and does it rather monotonically. The "passive" state of the qubit, state |01⟩, also receives some population during the pulse (up to ∼0.2), but at the end of the pulse its population is entirely transferred to the target state, so that this process is well controlled. The other "passive" state |00⟩ remains unpopulated for the reasons discussed above. Populations of the "interfering" states (in the vicinity of "computing" states of the two-qubit system) do not exceed 10^{-2} during the pulse, and they vanish almost entirely at $t = T$. During the last ∼ 3 ps of the pulse the field smoothly decreases and no population transfer occur.

The population dynamics during the other optimized transition, CNOT |11⟩ → |10⟩, is very similar to the CNOT|10⟩ → |11⟩ dynamics discussed in the previous paragraph, simply because these two processes represent the reverse of each other. Dynamics of the other two optimized transitions is simpler. Namely, if the initial qubit state is |00⟩ then all the populations remain almost unaffected by the pulse (within 2×10^{-3}), which is a trivial scenario for CNOT |00⟩ → |00⟩ consistent with discussion at the beginning of this section. If the initial state is |01⟩, the pulse induces some temporary excitation of |G⟩, |10⟩, and |11⟩ (up to ∼ 0.65), but it is returned back to |01⟩ at the end of the pulse, consistent with CNOT |01⟩ → |01⟩. Again, in all cases populations of the interfering states do not exceed 10^{-2} during the pulse action.

B. Effect of reduced bandwidth

The main goal of this work was to determine the requirements on frequency spectrum of the laser pulse (which also reflects requirements on characteristics of the pulse-shaper instrument) to achieve accurate and robust qubit transformations. In this section we study the effect of reducing bandwidth, by removing some of the frequency components from the optimized pulse. We do this by Fourier-transforming optimal pulse into frequency domain as discussed above, zeroing some of the amplitudes (at those frequencies that we want to remove), and Fourier-transforming the resultant filtered spectrum back to the time domain, producing new filtered laser pulse. Then, this new pulse is applied to the molecule in various initial states of the two-qubit system to perform four independent transitions of the CNOT gate, according to Eq. (1). For action of the filtered pulse the values of P and F are determined, and the time-dependent analysis of state populations is performed, in order to see the effect of modifications made.

TABLE II. Fidelities of CNOT gate for pulses with narrowed frequency range. First row shows results for the original optimized field without any filtering.

Left border (cm^{-1})	Right border (cm^{-1})	Number of frequency channels	Fidelity
1.35	200 231	150 000	0.999838
26 623	27 093	352	0.999838
26 815	26 895	64	0.999838
26 832	26 875	32	0.998953
26 845	26 862	13	0.846798

As mentioned above, the unfiltered optimized pulse contains 150 000 frequency components in a very broad, physically irrelevant frequency range (see 1st row of Table II). We tried to remove frequencies that do not contribute to qubit transformations by gradually narrowing frequency range of the pulse. Results of these tests are presented in Table II. First, we tried to keep only those frequency components that correspond to state-to-state transitions in our system—352 frequency components in the 470 cm^{-1} wide range (see 2nd row of Table II). As expected, no changes of P or F, or the underlying state-to-state dynamics were observed. Next, we tried to cut off more from the spectrum, leaving only 64 unchanged frequency channels around the central frequency. This part of spectrum corresponds to Fig. 2 and is only 80 cm^{-1} wide. The results are given in 3rd row of Table II and, again, are entirely identical to those of unfiltered optimal pulse. Note that this frequency range contains, besides four states of the two-qubit system, two "interfering" vibrational states—one on each side of the spectrum (green sticks in Fig. 2). In the next test we tried to remove even these two frequencies, reducing the number of frequency channels to just 32, which corresponds to the 43 cm^{-1} wide frequency range, shown in Fig. 4(a). Note that this modification cuts off two small spectral structures at the ends of the left and right wings of the optimized spectrum (see Fig. 4(a)). The results of this test are summarized in the 4th row of Table II, and we see that it leads to visible reduction of gate fidelity. This demonstrates quite clearly that controlling transitions to the interfering states is important if one wants to obtain very accurate quantum gates. In the final test of this series we tried to filter the spectrum as shown in Fig. 4(b), keeping only the intense peaks in the spectrum (13 frequency channels) and removing both wings entirely. The results, summarized in the 5th row of Table II, show a significant drop of gate fidelity. This was expected since we removed a number of frequency components with relatively high amplitudes, in particular from the low-frequency side of spectrum (see Fig. 4(b)). Still, the gate CNOT is meaningful ($F > 0.8$).

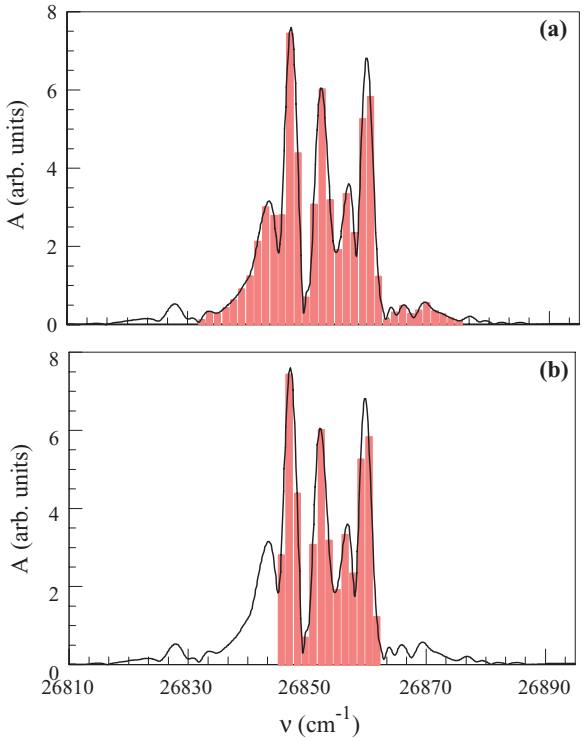

FIG. 4. Frequency content of the filtered pulses. Panel A shows the case of 32 frequency channels. Panel B shows the case of only 13 frequency channels kept.

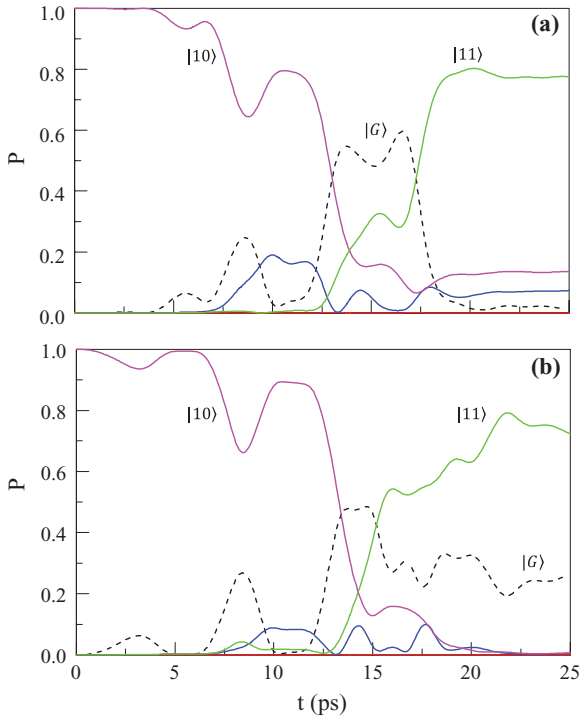

FIG. 5. Dynamics of state populations during transformation CNOT$|10\rangle \rightarrow |11\rangle$ of the two-qubit system. Panel A shows the case of 13 frequency channels. Panel B shows the case of phase rounding to 60° sectors. Blue and red lines show populations of states $|01\rangle$ and $|00\rangle$, respectively.

To gain further insight into the mechanism of fidelity loss in this test we analyzed the underlying population dynamics. The result for transition CNOT$|10\rangle \rightarrow |11\rangle$ is presented in Fig. 5(a), and can be directly compared to the high-fidelity 32-channels result of Fig. 3. In two cases the population dynamics is similar during the first half of the pulse. The difference starts showing up at about $t = 15$ ps, when the 13-channel case exhibits second increase of population of the gateway state. At the end of the pulse, in both cases, population of the gateway state is dumped onto the qubit states, but, in the 13-channel case some residual population is found in states $|10\rangle$ and $|01\rangle$, which explains low fidelity. Further analysis of the 13-channel case showed that no population has been transferred to the interfering states. This leads to conclusion that the erroneous population of the computing states of the two-qubit system is the main factor for fidelity loss in the case of the narrow-filtered pulse.

In the next series of tests we tried to understand the role of "wings" of the spectrum. For this purpose we filtered the optimized pulse by removing from the original spectrum either high-frequency or low-frequency components only. Namely, the frequency spectrum shows two small peaks and a wide wing on the low-frequency side; on the high-frequency side, the spectrum shows four weak narrow peaks (see Fig. 2(a)). We wanted to check the importance of each of these structures by filtering them out one by one, and applying such filtered pulses to the molecule in a manner described above. The results of this series of tests are summarized in Table III. Removing the low-frequency parts of spectrum maintains fidelity $F > 0.998$, up to the cut-off value of $\nu = 26\,835$ cm^{-1}, where the wide wing begins (see Fig. 2(a)). Removing this wing results in $F \sim 0.85$. Removing only a part of this structure still results in significant decline of fidelity. On the high-frequency side we performed more tests, due to larger number of minor peaks. Fidelity of the filtered pulse remains at the level $F > 0.998$, up to the cut-off value of $\nu = 26\,865$ cm^{-1}, when all but one minor peaks are removed. Removing this last peak reduces fidelity to $F \sim 0.96$. Therefore, we can conclude that most important is to keep one minor peak (adjacent to the major peak) on each side of the spectrum. Including the more remote peaks is important only if the fidelity in excess of $F \sim 0.998$ is desired.

On the practical side, it is very encouraging and is almost surprising that with only 64 frequency channels we are able to achieve (in calculations) highly-accurate quantum gate CNOT. In fact, even with 32 channels, when we control just transitions between states of the two-qubit system and ignore

TABLE III. Fidelities of CNOT gate for pulses with frequency range narrowed from one side.

Cutoff method	Cutoff frequency (cm^{-1})	Gate fidelity
Low frequency	26 830	0.999410
	26 835	0.998365
	26 845	0.852487
High frequency	26 880	0.999807
	26 875	0.999582
	26 868	0.998777
	26 865	0.998024
	26 862	0.960835

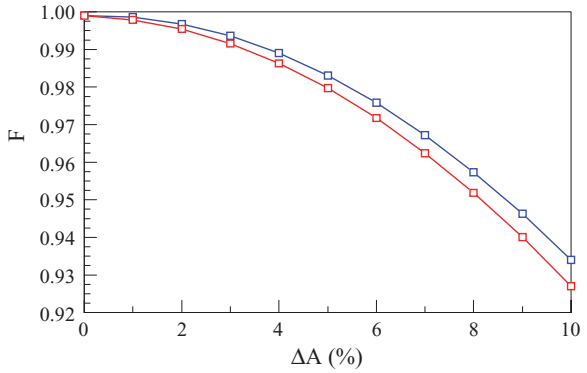

FIG. 6. Fidelity of CNOT gate as a function of deviation of pulse's amplitude from its optimal value. Blue and red symbols correspond to increased and decreased amplitudes, respectively.

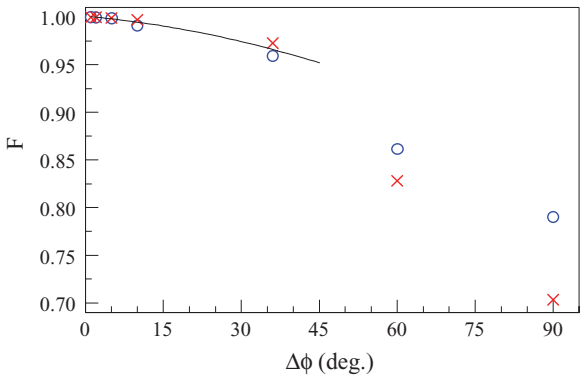

FIG. 7. Fidelity of CNOT gate as a function of phase rounding error. Blue and red symbols correspond to two different ways of rounding (see text for further details). Solid curve shows analytic fit by quadratic function.

the interfering transitions, we can achieve a reasonable gate fidelity, closely approaching $F = 0.999$, which is well sufficient for the first proof-of-principle experiment.

C. Effect of amplitude errors

The second goal of this work was to determine how sensitive the results of molecule-pulse interaction are to deviations of pulse's shape from the ideal optimal shape. The first parameter to study is pulse's amplitude. We tried to construct new modified pulses, from the optimal one, by changing the values of amplitudes of all frequency components simultaneously, by a given amount. Figure 6 illustrates the results of increasing and, alternatively, decreasing the amplitudes by up to 10% of the optimal values. We observed monotonic decrease of fidelity of the gate CNOT in both cases. The effect is well described by quadratic function,

$$F = 1 + a|\Delta A| - b|\Delta A|^2. \tag{11}$$

The values of fitting parameters are $a = 1.16 \times 10^{-4}$, $b = 6.65 \times 10^{-4}$ for positive ΔA and $a = 4.91 \times 10^{-4}$, $b = 6.75 \times 10^{-4}$ for negative ΔA values. For example, when the values of amplitudes are changed by 3%–4%, the fidelity stays relatively high, at the level of $F \sim 0.99$. Even a very significant deviation from the optimal amplitude, like by $\pm 10\%$ or so, still results in the meaningful results characterized by $F \sim 0.93$. Since both positive and negative deviations lead to similar decreases of gate fidelity, one could hope that a random noise (with both positive and negative deviations of amplitudes of different frequency components occurring simultaneously) will not lead to larger decrease of fidelity. To check this assumption we carried out a series of 50 additional calculations where the amplitude of each frequency component underwent random error in the range from -5% to $+5\%$ of its optimal value. These randomly modified pulses were independently applied to the molecule. The fidelity, averaged over 50 runs, was $F = 0.998416$ which is significantly higher than the values obtained with systematically positive ($F = 0.983093$ for $+5\%$ error) or systematically negative ($F = 0.979696$ for -5% error) values. Thus, the results presented in Fig. 6 can be considered as "the worst case scenario" and serve as lower bound for estimation of fidelity loss due to amplitude errors.

D. Effect of phase errors

The last question to explore is the effect of phase errors. For this purpose we took the values of phases of different frequency components of the optimized pulse (see Fig. 2(b)), and tried to modify them by rounding their values to a set of discrete equally spaced values in the range $-180^\circ < \varphi < +180^\circ$. The coarseness of phase rounding in our tests varied from only $\Delta\varphi = 1^\circ$ up to $\Delta\varphi = 90^\circ$ (see Fig. 7). Rounding phases of the optimized pulse components introduces phase errors. For example, for $\Delta\varphi = 30^\circ$ the optimal phases are modified by up to $\pm 15^\circ$. Using the intrinsic routine NINT( ) of FORTRAN this rounding operation would be written as

$$\bar{\varphi} = \Delta\varphi \cdot \mathrm{NINT}(\varphi/\Delta\varphi), \tag{12}$$

where φ is the optimized value of phase and $\bar{\varphi}$ is value of phase after rounding.

When the rounding is very coarse it becomes important which discrete values of phases are chosen. For example, for $\Delta\varphi = 90^\circ$ one can chose $\varphi = \{-90^\circ, 0^\circ, 90^\circ, 180^\circ\}$ or, alternatively, the values of $\varphi = \{-135^\circ, -45^\circ, 45^\circ, 135^\circ\}$ obtained from the first set through $\Delta\varphi/2$ rotation. So, we tried both methods of rounding for each studied value of $\Delta\varphi$.

Our results for gate CNOT are summarized in Fig. 7. We see that as $\Delta\varphi$ increases, the value of gate fidelity F gradually drops. For example, relatively large phase errors introduced by $\Delta\varphi = 30^\circ$ lead to only modest decrease of fidelity, down to $F \sim 0.97$. In the high fidelity region of Fig. 7 the results of simulations can be approximated by a quadratic function of the form

$$F = 1 - a \cdot \Delta\varphi - b \cdot (\Delta\varphi)^2 \tag{13}$$

with $a = 4.88 \times 10^{-4}$, $b = 1.32 \times 10^{-5}$.

When phases of frequency components of the optimal pulse are modified, the dynamics of state-to-state transitions also changes. Figure 5(b) illustrates this effect in the case of $\Delta\varphi = 60^\circ$, for transition CNOT$|10\rangle \rightarrow |11\rangle$. This figure can be compared to Figs. 3 and 5(a). The effect of phase errors (Fig. 5(b)) is different from the effect of reduction of number of frequency channels (Fig. 5(a)). Interestingly, phase errors lead to residual population of the gateway state $|G\rangle$ and reduced population of the target state $|11\rangle$, while populations

of states $|01\rangle$ and $|10\rangle$ (and of the interfering states) are all accurately controlled.

V. CONCLUSIONS

The purpose of this computational work is exploratory, rather than predictive. We do not really expect that the CNOT pulse obtained here by calculations can be exactly reproduced in the experiment and can lead to exactly the same result under experimental conditions. However, we feel it is reasonable to expect that employment of an advanced experimental pulse optimization technique, such as feedback loop with evolutionary algorithm, may lead to experimental result of acceptable quality. Computational results outlined in this paper could serve as prediction of a reasonable set of requirements for the pulse spectrum and, consequently, for the pulse shaping equipment. We found that the number of frequency channels needed for accurate two-qubit gate is not large. Calculations showed that 32 frequency channels may be well sufficient for moderate fidelity of qubit transformations, $F \sim 0.999$. This result is reliable, because it is based on realistic experimental spectrum and transition moments of thiophosgene. If the frequency resolution Δv (defined by the pulse length T) is kept fixed, increasing the number of channels beyond 32 is not expected to be beneficial. However, it may be beneficial to increase the number of frequency components (within the same bandwidth) simultaneously with improving frequency resolution Δv. Effect of pulse shaping errors was studied separately for amplitudes and phases of frequency components. Moderate errors in amplitudes (within $\pm 4\%$ of the optimal values) and phases (within $\pm 5^\circ$ of the optimal values) are not expected to reduce fidelity of qubit transformations below $F \sim 0.99$, indicating favorable path to experimental implementation.

In calculations, such laser pulses can be readily constructed using OCT. Although the OCT has a huge bandwidth initially available for pulse construction, and there are no any constraints on use of this bandwidth, the optimal pulses come out restricted to surprisingly small bandwidth. The most intense frequency components are resonant to frequencies of controlled transitions, but the off-resonant wings on both sides of spectrum appear to be important for accurate qubit transformations. Transitions to energetically remote interfering states are simply avoided by OCT, through suppressing field amplitude at the corresponding frequencies, which is probably the main reason for small bandwidth of the optimized pulses. When we tried to limit the original bandwidth (manually, in the frequency domain) to only 64 frequency channels, we did not observe any decay of the pulse fidelity at the level of six significant figures: the gate average probability of CNOT remained at the level of >0.9999, while the phase sensitive gate fidelity was very close to this value. This does bode well for robust solutions.

ACKNOWLEDGMENTS

This work was supported by the National Science Foundation, Grant No. CHE-1012075. This research used resources of the National Energy Research Scientific Computing Center, which is supported by the Office of Science of the U.S. Department of Energy under Contract No. DE-AC02-05CH11231. Professor Martin Gruebele at the University of Illinois at Urbana-Champaign is acknowledged for fruitful discussions.

[1] W. Zhu, J. Botina, and H. Rabitz, J. Chem. Phys. **108**, 1953 (1998).
[2] W. Zhu and H. Rabitz, J. Chem. Phys. **109**, 385 (1998).
[3] H. Rabitz, M. Hsieh, and C. Rosenthal, Science **303**, 1998 (2004).
[4] E. Berrios, M. Gruebele, D. Shyshlov, L. Wang, and D. Babikov, "High fidelity quantum gates with vibrational qubits," J. Phys. Chem. (to be published).
[5] H. Rabitz, R. de Vivie-Riedle, M. Motzkus, and K. Kompa, Science **288**, 824 (2000).
[6] A. Assion, T. Baumert, M. Bergt, T. Brixner, B. Kiefer, V. Seyfried, M. Strehle, and G. Gerber, Science **282**, 919 (1998).
[7] R. Bartels, S. Backus, E. Zeek, L. Misoguti, G. Vdovin, I. P. Christov, M. M. Murnane, and H. C. Kapteyn, Nature (London) **406**, 164 (2000).
[8] D. Weidinger and M. Gruebele, Mol. Phys. **105**, 1999 (2007).
[9] R. R. Zaari and A. Brown, J. Chem. Phys. **135**, 044317 (2011).
[10] W. Zhu and H. Rabitz, J. Chem. Phys. **118**, 6751 (2003).
[11] J. P. Palao and R. Kosloff, Phys. Rev. Lett. **89**, 188301 (2003).
[12] J. P. Palao and R. Kosloff, Phys. Rev. A **68**, 062308 (2003).
[13] C. M. Tesch, L. Kurtz, and R. de Vivie-Riedle, Chem. Phys. Lett. **343**, 633 (2001).
[14] C. M. Tesch and R. de Vivie-Riedle, Phys. Rev. Lett. **89**, 157901 (2002).
[15] U. Troppmann, C. M. Tesch, and R. de Vivie-Riedle, Chem. Phys. Lett. **378**, 273 (2003).
[16] C. M. Tesch and R. de Vivie-Riedle, J. Chem. Phys. **121**, 12158 (2004).
[17] B. Korff, U. Troppmann, K. Kompa, and R. de Vivie-Riedle, J. Chem. Phys. **123**, 244509 (2005).
[18] U. Troppmann and R. de Vivie-Riedle, J. Chem. Phys. **122**, 154105 (2005).
[19] U. Troppmann, C. Gollub, and R. de Vivie-Riedle, New J. Phys. **8**, 100 (2006).
[20] Z. Amitay, R. Kosloff, and S. R. Leone, Chem. Phys. Lett. **359**, 8 (2002).
[21] D. Babikov, J. Chem. Phys. **121**, 7577 (2004).
[22] J. Vala, Z. Amitay, B. Zhang, S. R. Leone, and R. Kosloff, Phys. Rev. A **66**, 062316 (2002).
[23] Y. Ohtsuki, Chem. Phys. Lett. **404**, 126 (2005).
[24] S. Suzuki, K. Mishima, and K. Yamashita, Chem. Phys. Lett. **410**, 358 (2005).
[25] Y. Teranishi, Y. Ohtsuki, K. Hosaka, H. Chiba, H. Katsuki, and K. Ohmori, J. Chem. Phys. **124**, 114110 (2006).
[26] D. Weidinger and M. Gruebele, Chem. Phys. **350**, 139 (2008).
[27] T. Cheng and A. Brown, J. Chem. Phys. **124**, 34111 (2006).
[28] M. Schröder and A. Brown, J. Chem. Phys. **131**, 034101 (2009).
[29] R. R. Zaari and A. Brown, J. Chem. Phys. **132**, 014307 (2010).
[30] R. R. Zaari and A. Brown, J. Chem. Phys. **137**, 104306 (2012).
[31] M. Zhao and D. Babikov, J. Chem. Phys. **126**, 204102 (2007).
[32] Y. Y. Gu and D. Babikov, J. Chem. Phys. **131**, 034306 (2009).
[33] B. Strickler and M. Gruebele, Phys. Chem. Chem. Phys. **6**, 3786 (2004).
[34] T. Laarmann, I. Shchatsinin, P. Singh, N. Zhavoronkov, M. Gerhards, C. P. Schulz, and I. V. Hertel, J. Chem. Phys. **127**, 201101 (2007).
[35] M. Kotur, T. Weinacht, B. J. Pearson, and S. Matsika, J. Chem. Phys. **130**, 134311 (2009).
[36] A. Nemeth, F. Milota, T. Mančal, V. Lukeš, J. Hauer, H. F. Kauffmann, and J. Sperling, J. Chem. Phys. **132**, 184514 (2010).
[37] A. du Plessis, C. A. Strydom, H. Uys, and L. R. Botha, J. Chem. Phys. **135**, 204303 (2011).
[38] M. A. Nielsen and I. L. Chuang, *Quantum Computation and Quantum Information* (Cambridge University Press, Cambridge, 2000).
[39] M. Zhao and D. Babikov, J. Chem. Phys. **125**, 024105 (2006).
[40] M. Zhao and D. Babikov, Phys. Rev. A **77**, 012338 (2008).
[41] L. Wang and D. Babikov, Phys. Rev. A **83**, 022305 (2011).
[42] L. Wang and D. Babikov, Phys. Rev. A **83**, 052319 (2011).
[43] L. Wang and D. Babikov, J. Chem. Phys. **137**, 064301 (2012).
[44] J. I. Cirac and P. Zoller, Phys. Rev. Lett. **74**, 4091 (1995).
[45] D. M. Meekhof, C. Monroe, B. E. King, W. M. Itano, and D. J. Wineland, Phys. Rev. Lett. **76**, 1796 (1996).
[46] K. Sundermann and R. de Vivie-Riedle, J. Chem. Phys. **110**, 1896 (1999).